Sustainable Materials and Technologies 32 (2022) e00399

Contents lists available at ScienceDirect

Sustainable Materials and Technologies

journal homepage: www.elsevier.com/locate/susmat

A cycling-insensitive recycling method for producing lithium transition metal oxide from Li-ion batteries using centrifugal gravity separation

Ruiting Zhan, Lei Pan *

Department of Chemical Engineering, Michigan Technological University, 1400 Townsend Drive, Houghton, MI 49931, United States

ARTICLE INFO

Keywords:
Li-ion battery recycling
Centrifugal gravity separation
Falcon ultra-fine (UF) separator
Black mass
Cathode active materials
Lithium transition metal oxides

ABSTRACT

The separation and recovery of electrode active materials from Li-ion batteries is a requisite step prior to any downstream hydrometallurgical and direct recycling processes. Prior research efforts into the separation between the two electrode active materials from Li-ion batteries was limited to the froth flotation process; however, any changes to the surface properties of the active materials resulted in an inferior separation performance. In this work, a novel separation method, namely the Falcon Ultra-Fine (UF) centrifugal gravity concentration, is developed to separate electrode active materials from Li-ion batteries. Results obtained with a mixture of pristine lithium transition metal oxides (LTMOs) and graphite showed that the separation between the two materials perform well with over 90% of LTMOs in the concentrate product after one pass in the UF concentrator. Multiple stages of the separation processes enabled a concentration of LTMOs with 99% purity. Results obtained with aged electrode active materials from spent Li-ion batteries showed that the concentrate product consisted of at least 98% by weight of LTMOs. It was observed that there was a misplacement of LTMOs in the overflow product, which was attributed to the presence of ultrafine LTMOs as well as PVDF-binded cathode agglomerates in the feed. Results of this work demonstrate a viable method for separating mixed electrode active materials and producing high-purity LTMOs, which can be potentially used for the direct recycling of cathode active materials in the manufacturing of new Li-ion batteries.

1. Introduction

Lithium-ion (Li-ion) batteries, commercialized in 1990 by Sony, have become the state-of-the-art technology for energy storage due to their high energy density and long cycling life [1–3]. Li-ion batteries contain ~50% by weight of critical and strategic minerals including lithium, nickel, cobalt, manganese, and graphite [4–6]. Battery recycling is an integral part of environmental stewardship for energy storage and electric vehicle (EV) businesses, and in many countries, the recycling of Li-ion batteries is mandatory. Since Li-ion batteries contain hazardous and flammable materials [7–9], the recycling of flammable electrolyte solvents reduces the amount of hazardous materials entering the environment. Recycling and reuse of battery materials from spent Li-ion batteries is essential for the sustainable pursuit of renewable green energy resources [10,11].

Three recycling methods for spent Li-ion batteries have been developed, namely the pyrometallurgical, the hydrometallurgical, and the direct recycling methods [12]. Both the pyrometallurgical and hydrometallurgical processes are designed to recover valuable metals such as cobalt and nickel. Direct recycling separates and recovers both anode active materials (*i.e.* graphite) and cathode active materials (*i.e.* lithium transition metal oxides, LTMO) from Li-ion batteries without changing their structure and chemistry during the recycling process [9]. In the direct recycling process, battery cells are disassembled and crushed into individual battery components. Solvents within Li-ion batteries evaporate at room temperature due to their high vapor pressure, leaving behind dry electrode sheets. Various size separation and gravity separation processes have been developed to separate battery components [13–15]. When the electrode active powder materials are delaminated from the current collectors, the fine fraction of the crushed Li-ion batteries consists of anode and cathode active materials, while the coarse fraction consists of current collectors, *e.g.,* Cu and Al, and plastics. Graphite is commonly used as the anode active material, while lithium transition metal oxides (LTMO), *e.g.,* lithium nickel manganese cobalt oxide ($LiNi_xMn_yCo_zO_2$, $x + y + z = 1$, NMC), are used as the cathode active material. The recycled active materials must be relithiated and repaired prior to re-use in new Li-ion batteries [16–22].

Separating anode and cathode active materials from Li-ion batteries

* Corresponding author at: 1400 Townsend Drive, Houghton, MI 49931, United States.
E-mail address: leipan@mtu.edu (L. Pan).

https://doi.org/10.1016/j.susmat.2022.e00399
Received 26 September 2021; Received in revised form 16 January 2022; Accepted 23 January 2022
Available online 29 January 2022
2214-9937/Published by Elsevier B.V.

is required prior to any direct recycling and chemical refining processes. Prior R&D efforts were devoted to the use of froth flotation as the recycling method [23–25]. Froth flotation separates mixed materials by taking advantage of the difference in surface hydrophobicities between the graphite and lithium transition metal oxide (LTMO) materials. Graphite is hydrophobic, while metal oxide is hydrophilic. Air bubbles carry hydrophobic graphite particles to the froth layers, leaving hydrophilic metal oxide materials in the slurry [23]. Separation occurs when particle-loaded froth flows into the launder. For lightly used EV batteries, anode active materials remain hydrophobic, and consequently all anode materials are floated with a kerosene collector. A good separation between the anode and cathode active materials is achieved [26]. For severely degraded Li-ion batteries, electrolyte degradation results in the formation of an oxygen-rich, solid electrolyte interphase (SEI) layer on the anode surface, rendering the surface hydrophilic [27]. Consequently, the anode materials become difficult to float. In addition, the exposure of both PVDF binders and carbon additives results in an unfavorable flotation of cathode agglomerates. It has been shown that the separation between the anode and cathode active materials from end-of-life Li-ion batteries improved after a thermal treatment process [24,25]. This thermal treatment process effectively removed the SEI layers, rendering the surface of the anode active materials hydrophobic [24]. In addition, this thermal process removed PVDF binders, enhancing the surface hydrophilic property of the cathode active materials. Alternatively, an improvement in the froth flotation separation has been achieved using a fine grinding that exposed fresh surfaces of the aged anode active materials [28].

Gravity separation between the anode and cathode active materials has also been previously investigated [29,30]. Various heavy liquids were used to separate the anode active materials from the cathode active materials [29,30]. Cathode active materials, *e.g.,* lithium cobalt oxide (LCO) and lithium nickel manganese cobalt oxide ($LiNi_xMn_yCo_zO_2$, $x + y + z = 1$), with density of 4.5–5.0 g/cm^3, are much denser than graphite having density of 2.26 g/cm^3. Therefore, heavy liquids having densities in the range of 2.26–4.50 g/cm^3 enable a separation between the two mixed materials [31]. Diiodomethane, bromoform, sodium polytungstate (SPT), and lithium metatungstate (LMT) may be used for this purpose. However, these heavy liquids are viscous, and thereby prohibit the use in the industrial settings. In addition, organic heavy liquids are toxic, and the recycling of these heavy liquids is challenging [32]. The separation of the two electrode active materials from Li-ion batteries was studied using a Falcon Semi-Batch (SB) concentrator operating at 10–150 G forces [33]. Up to 80% purity of cathode active materials in the underflow (concentrate) product was obtained at a recovery of approximately 50% [34]. To date, no satisfactory separation performance has been achieved.

Both the anode and cathode active materials used in Li-ion batteries have particle sizes of 5–20 μm. The Falcon Ultra-Fine (UF) concentrator is a centrifugal gravity separation method that potentially can be used to separate such ultrafine particles [35]. This concentrator is used for concentrating platinum group metals (PGM), gold, and silver from an ultrafine ore feed [36–38]. In this study, separation between the two electrode active materials used in Li-ion batteries by the Falcon UF concentrator is evaluated using a blended mixture of pristine graphite and lithium nickel-manganese-cobalt oxide, as well as black mass (*i.e.,* a mixture of the two electrode active materials) from spent Li-ion batteries. The results are analyzed to determine two key metrics: the separation index (SI) and the grade of lithium transition metal oxides (LTMO) in the concentrate product. Both the single-stage and multi-stage experiments were conducted.

2. Materials and methods

2.1. Materials

Pristine lithium nickel manganese cobalt oxide NMC111 ($LiNi_{0.33}Mn_{0.33}Co_{0.33}O_2$) was obtained from Toda America, and pristine graphite (SLC1520P) powders were obtained from Superior Graphite. De-ionized (DI) water, with a resistance of 17.9–18.2 MΩ·cm, was obtained from a Barnard water purification system (Thermo Fisher). Lithium metatungstate (LMT), with a specific density of 2.95, was obtained from LMT Liquid Inc. and was used as received.

Spent Li-ion batteries were removed from used Laptop battery packs (Michigan Tech IT as well as various battery recyclers in the United States). They were discharged to 2.8 V at a C/10 rate and held at 2.8 V for at least 24 h prior to being dismantled. The battery cells were opened using a rotary tool to remove stainless-steel casing. The battery cores were then unfolded to manually separate anode layers, cathode layers, plastic separators, and other components. The unfolding process was performed under a fume hood to evaporate volatile organic solvent residues. The anode, cathode, and separator layers were cut and shredded to approximately 0.5″ x 0.5″ pieces and fed into a blender filled with DI water. The delamination process was carried out using a wet agitation method in a 1-L commercial blender running at 6000–10,000 RPM. An agitation time of 5–30 s was sufficient to delaminate 95% of the electrode active materials from the current collectors. Using an appropriate agitation time, the majority of the electrode active materials were in a size fraction of less than 100 μm, while the majority of the current collectors (Al, Cu, and plastics) were in a size fraction of above 500 μm. The slurries were then sieved using a 70-mesh screen, rinsed with DI water three times, and filtered to obtain wet filter cakes. The resulting black mass mostly consisted of graphite and lithium transition metal oxide powders.

2.2. Separation mechanism

Fig. 1 shows a schematic drawing of the Falcon ultrafine (UF) concentrator used in this study. The Falcon UF concentrator is a conical smooth bowl with a slight reduction in diameter at the outlet to create a retention zone [39]. The UF concentrator has a depth of 4.13 in. and an inner diameter of 4.00 in. The bowl rotates up to 4800 RPM, creating a centrifugal force in the range of 50G - 300G. The UF concentrator consists of two sections including 1) a migration zone and 2) a retention zone [39]. At the migration zone, the slurry forms a liquid film with particles preferentially concentrated along the wall of the rotating bowl, creating strong interlayer shears under the centrifugal force. Due to the difference in particle settling velocities, fine heavy particles arrive at the wall prior to coarse light ones. As the slurry continues to feed into the bowl, more particles compact along the wall of the rotating bowl. Coarser, denser particles move across the interlayers, then into its inner

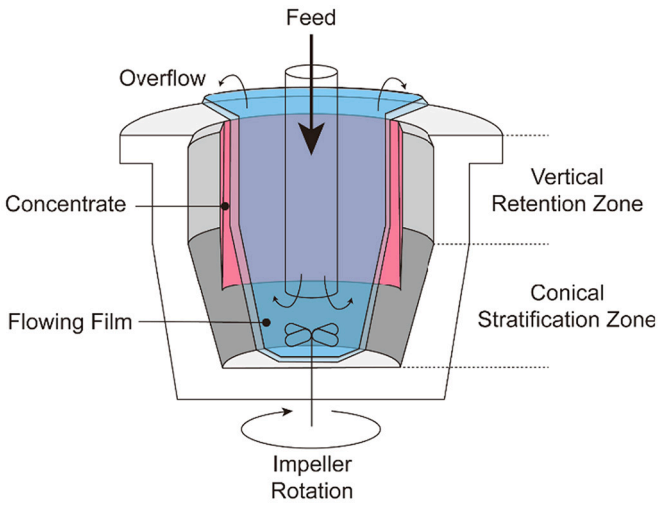

Fig. 1. A schematic cross-sectional drawing of the Falcon ultrafine (UF) concentrator after Refs [35, 41].

wall, pushing smaller and lighter particles out of the bed. These lighter and smaller particles are flushed with the overflow stream, and reported to the overflow product [40]. Particles at the retention zone are then collected manually in a laboratory setting or by flushing with water into an underflow product in commercial operations.

2.3. Experimental procedure

In this study, separation between the lithium metal oxide and graphite was conducted using a Falcon L40 ultrafine (UF) concentrator. The two materials were mixed with DI water at different weight ratios to prepare a slurry. The slurry was agitated using an overhead agitator (Caframo) to ensure that the slurry was well mixed. In a nominal operation, the slurry was fed through a center feed tube of the rotating concentrator, at a feed rate of approximately 3.0 L/min. Rotation ceased when the slurry was no longer able to flush into the overflow stream, and the materials inside the concentrator were sampled, collected, and dried in an oven overnight at 100 °C. All samples were weighted, and a fraction of these samples were analyzed using thermogravimetric analysis (TGA) to obtain the materials' composition.

2.4. Data analysis

Two sampling methods were used to evaluate the separation performance. In the first sampling method, materials collected inside the bowl were used as the heavy concentrate product, while the overflow slurry was used as the light tailing product. The separation index (SI) is defined as the recovery of cathode active materials (R_C) in the concentrate minus the recovery of anode active materials (R_A) in the concentrate, as $SI = R_C - R_A$. An SI value equal to 1 suggests a 100% separation between the two electrode active materials, while an SI equal to 0 means there was no separation between the two materials. A SI of 0.6 may suggest that 80% of NMC and 20% of graphite from the feed in the concentrate product. The second sampling method aims to maximize the percentage of cathode active materials in the concentrate product. In the second sampling method, wet materials deposited at 3 cm below the top edge of the concentrator were collected as the heavy concentrate product. The rest of materials within the bowl, combined with the overflow product, were collected as the tailing product. Both the SI value and the recovery and grade of lithium transition metal oxides in the concentrate product were then determined.

2.5. Characterization

Material compositions were analyzed using the thermogravimetric analysis (TGA) method, using an automatic thermogravimetric analyzer (TGA701, LECO). The chamber temperature rose from room temperature to 800 °C, with a rate of 1 °C/min. The measurements were conducted at an air flow of 7 L/min. The remaining mass percentage of the sample at 800 °C was the mass percentage of LTMO in the sample, while the percentage of the weight loss was the percentage of graphite in the sample. Both the chemical composition and morphology of the samples were determined using scanning electron microscopy (SEM) coupled with energy-dispersive X-ray spectroscopy (EDX). Imaging and elemental mapping was performed in a Philips XL40 environmental scanning electron microscope (ESEM) at 15 kV accelerating voltage in high vacuum. Images were obtained under back scattered electron (BSE) mode.

3. Results

3.1. Material characterization

To evaluate the separation performance of the Falcon UF concentrator, a mixture of pristine anode and cathode active materials, *i.e.*, graphite and NMC111, was first used as the feed. Fig. 2a shows the particle size distribution (PSD) by volume for both the pristine NMC111 and the graphite materials. The mean particle sizes of the pristine NMC and graphite materials were 9.23 and 18.22 μm, respectively. As shown, the graphite particles were slightly bigger than the NMC111 powders. Fig. 2b shows an image of a mixture of pristine NMC111 and graphite in the LMT solution in 2 days after mixing. Graphite powders floated to the

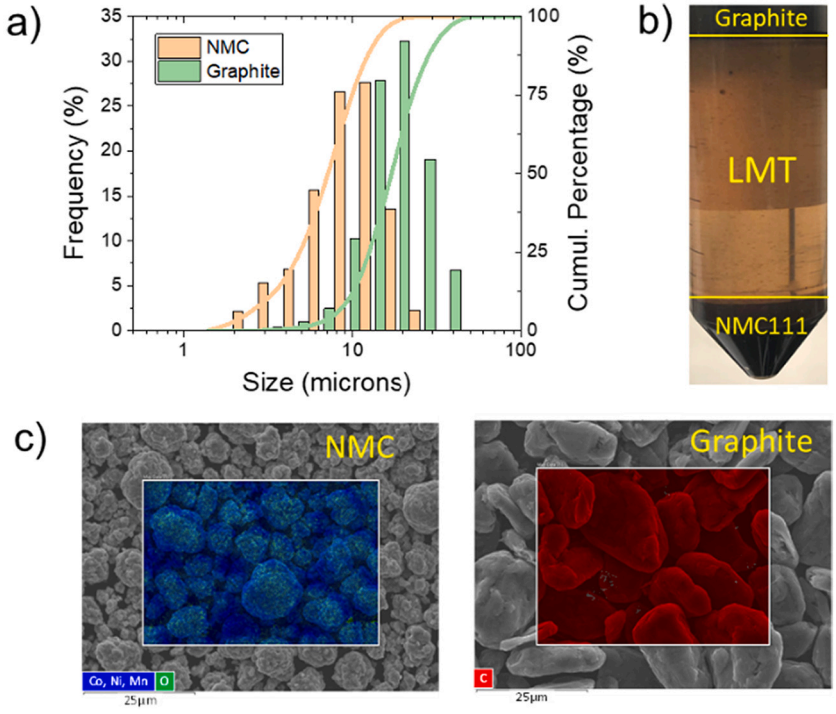

Fig. 2. a) Particle size distribution (PSD) of graphite and lithium nickel manganese cobalt oxide (NMC111) materials, b) a photo of a mixture of graphite and NMC111 powders in a lithium metatungstate (LMT) solution after settling in 2 days, and c) SEM and EDX mapping images of NMC111 and graphite materials.

surface of the LMT solution while NMC111 sunk to the bottom, confirming the difference in specific densities between these two materials. Fig. 2c shows SEM/EDX images of the NMC111 and graphite particles. Both particles were spherical, with graphite particles slightly larger than NMC111 particles.

3.2. Separation between pristine graphite and NMC111

Table 1 shows both the yield and composition of both the concentrate and tailing products after one pass in the Falcon UF concentrator, operating at 163 G force (60 Hz). Semi-wet materials deposited along the inner surface of the bowl were collected as the concentrate product, while the overflow slurry was collected as the tailing product. A 6-l slurry consisting of 180 g of NMC111 and 120 g of graphite was fed to the concentrator. The results showed that 67% of the solid materials was collected within the concentrator, and the remaining 33% was rejected to the tailing product. The concentrate product consisted of 86.48% of NMC and 13.52% of graphite by weight, while the tailing product consisted of 87.75% of graphite and 12.25% of NMC by weight. The yield (or recovery) of NMC in the concentrate product reached 93.78%, while the yield of graphite in the concentrate product was 24.76%. The separation index (SI) was determined to be 69.02%. Overall, a good separation performance was achieved after one pass in the UF concentrator.

Fig. 3 shows the effect of feed mass on the separation between pristine NMC111 and graphite, with detailed experimental data shown in Table 2. This result was obtained with 100 to 600 g of solid materials having a 60:40 NMC:C ratio by weight mixed in 5 wt% slurries. This experiment operated at 163 G force. The results showed that the yield of the concentrate product decreased with increasing the feed mass monotonically (Fig. 3a). Fig. 3b shows the percentage (or grade) of NMC in both the concentrate and tailing products at different feed masses. The results showed that the grade of NMC in the concentrate product increased with increasing the feed mass. For instance, the grade of NMC in the concentrate product increased from 65.46% with 100 g of the dry feed to 90.82% at 600 g of the dry feed. The grade of NMC in the tailing product was decreased from 20.40% at 100 g of the dry feed to 11.25% at 400 g of the dry feed, but increased to 18.23% at 600 g of the dry feed. This result showed that 500–600 g of dry feed were desirable for maximizing the grade of NMC in the concentrate product.

Fig. 3c shows the recovery of both the NMC and graphite in the concentrate product at different feed masses. At 100 g of the dry feed, although the recovery of the NMC in the concentrate was 97.20%, the recovery of graphite in the concentrate product was 82.43%. This yields a separation index of 14.77%, suggesting a poor separation between NMC and graphite. By increasing the feed mass, the recovery of NMC111 in the concentrate product dropped slightly, but the recovery of graphite in the concentrate product increased with increasing the feed mass. For instance, the recovery of graphite in the concentrate product dropped from 82.43% at 100 g of the dry feed to 12.71% at 600 g of the dry feed. Since the separation index is the difference in the recovery between the NMC and graphite in the concentrate product, the separation index (SI) increased with increasing the feed mass and reached a plateau of 75.38% at 500 g of the dry feed. At 600 g of the dry feed, the separation index (SI) dropped slightly to 73.90% due to a lower yield (86.61%) of NMC in the concentrate product. The decrease in the separation performance at the higher feed mass may be attributed to an overloading of the heavy materials in the concentrator. For NMC materials with a mean particle size (P50) of 9.23 μm, the maximum concentrate loading was approximately 300 g.

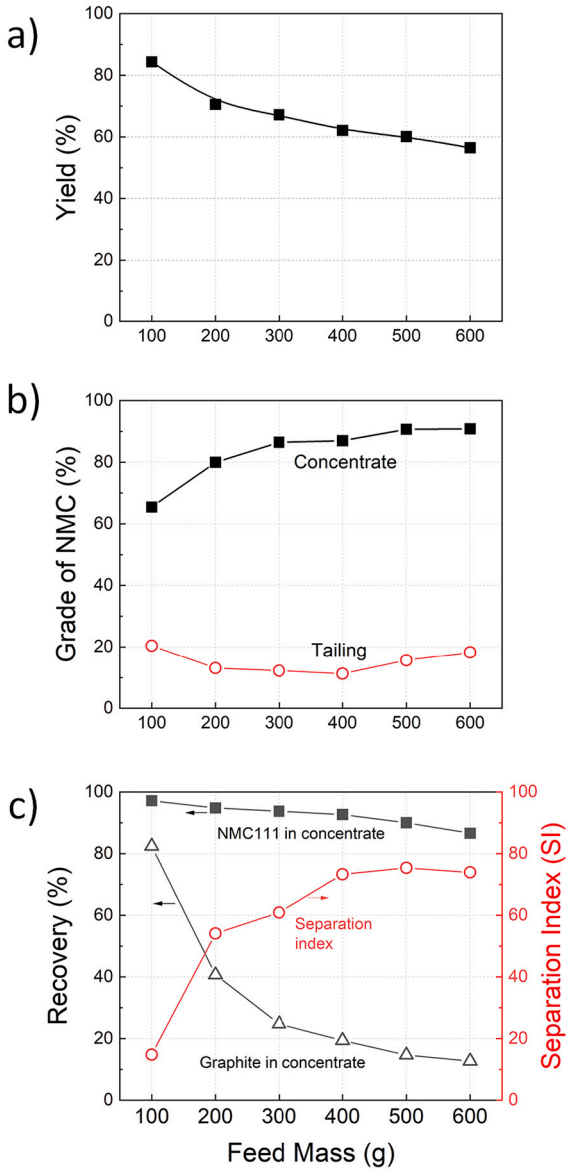

Fig. 3. Effect of feed mass on the separation between the NMC111 and graphite materials. a) yield or mass of the concentrate products at different feed masses, b) the percentage (or grade) of NMC111 in the concentrate and tailing products, c) recovery of NMC111 in the concentrate and tailing products as well as the separation index.

Fig. 4 shows the effect of g-forces on the separation between the NMC and graphite. The feed was a 5 wt% slurry with 400 g of the solid materials having a 3:2 NMC-to-graphite ratio by weight. Experiments were conducted at different g-forces in the range of 41 G – 290 G. The result showed that the yield of the NMC in the concentrate product increased

Table 1
Separation between the pristine NMC111 and graphite in a 5% solid slurry after one pass in Falcon Ultra-Fine (UF) concentrator operating at 163 g-force.

Product	Mass (g)	Yield (%)	Composition		Distribution (%)	
			NMC (%)	C (%)	NMC (%)	C (%)
Concentrate	201.55	67.18%	86.48%	13.52%	93.78%	24.76%
Tailing	94.32	32.82%	12.25%	87.75%	6.22%	75.34%
Feed	295.87	100.00%	62.82%	37.18%	100.00%	100.00%

Table 2
Effect of feed mass on the separation between the NMC and graphite in the concentrate and tailing products.

Feed mass (g)	Mass of Conc (g)	Yield of Conc (%)	Recovery of NMC in Conc	Recovery of graphite in Conc	Separation index	Grade of NMC (%NMC) in Conc	Grade of NMC (%NMC) in Tail
100 g	84.35 g	84.35%	97.20%	82.43%	14.77%	65.46%	20.40%
200 g	141.11 g	70.55%	94.82%	40.69%	54.13%	79.96%	13.10%
300 g	201.55 g	67.18%	93.78%	24.76%	60.92%	86.48%	12.25%
400 g	264.04 g	62.12%	92.69%	19.39%	73.30%	86.98%	11.25%
500 g	303.75 g	60.09%	90.03%	14.66%	75.38%	90.70%	15.64%
600 g	337.37 g	56.48%	86.61%	12.71%	73.90%	90.82%	18.23%

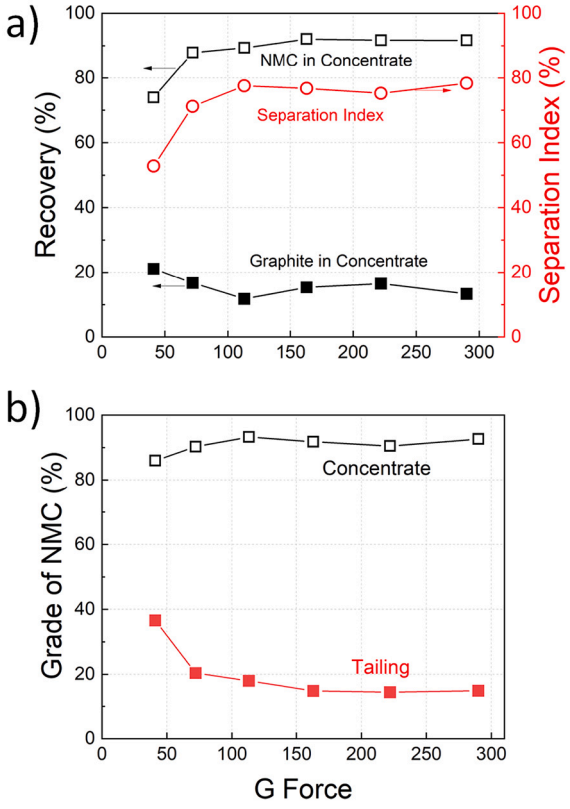

Fig. 4. Effect of g-force on the separation between the NMC and graphite. a) recovery of NMC and graphite in the concentrate as well as the separation index at different G forces; b) grade of NMC in both the concentrate and tailing products.

with increasing g-forces, and reached a plateau at 113 G or higher, while the yield of graphite in the concentrate product decreased with increasing g-forces. The separation index increased from 52.80% at 41–72 G to 76–78% at 113–290 G. The present finding suggests that the impact of g-force was marginal on the separation index at g-forces above 113 G.

Fig. 4b shows the grade of NMC in both the concentrate and tailing products. The percentage of NMC in the concentrate product reached 91–93% at 113–290 G after one pass in the UF concentrator. On the contrary, the grade of NMC in the tailing product decreased from 36.61% at 41 G to 14.49–14.88% at 163–290 G. It was noticed that the percentage of the NMC in the concentrate increased by increasing g-force, while the percentage of NMC in the tailing decreased by increasing g-force.

Fig. 5 shows the effect of solid concentration on the separation between the NMC and graphite. The feed consisted of 300 g and 400 g of the solid mixture having a 60:40 NMC-to-graphite ratio by weight. The solid concentration in the slurry ranged from 2.5% to 20%. For both 300 and 400 g of dry feed mass, the recovery of NMC in the concentrate product increased with increasing solid concentrations. Furthermore, the recovery of graphite in the concentrate product increased with increasing the solid concentrations in the slurry. At 15% solid concentration or higher, there was a substantial increase in the recovery of graphite in the concentrate product compared to that obtained at 10% solid concentration or less.

Fig. 5b shows the separation index at different solid concentrations. The separation index (SI) increased with increasing the solid concentrations, reached a plateau at 10% solid concentration, and decreased with further increasing the solid concentration. As shown, with 300 g of dry feed, the optimum separation index was 76.12% obtained at 10% solid concentration. The same conclusion was reached with 400 g of dry feed. At low solid concentrations, heavy particles were easily flushed with the slurry into the overflow stream, resulting in a decrease in recovery of the NMC in the concentrate. At high solid concentrations, graphite particles were trapped between interlayers within the particle bed, resulting in a poor separation between the graphite and NMC.

Solid concentration was also found to be sensitive to the grade of NMC in both the concentrate and tailing products. The result (Fig. 5c) showed that the percentage of NMC in the concentrate product was relatively the same at 10% solid concentration or less. However, as the solid concentration increased, the percentage of NMC in the tailing product decreased. As shown, with 300 g of the dry feed, the grade of NMC in the tailing product decreased from 17.8% at 2.5% solid concentration to 11.3% at 10% solid concentration. This result suggested that a high solid loading within the concentrator prevents particle movement between the interlayers within the particle bed, resulting in poor stratification and separation.

The effect of feed composition on the separation performance was also examined. The 60:40 NMC-to-graphite ratio by weight is a ratio between the two electrode active materials in the black mass from Li-ion batteries. After one pass in the UF concentrator, the tailing product contained 10–30% of NMC111 by weight. The remaining NMC materials in the tailing product were to be recovered to maximize the overall recovery. Fig. 6 shows the result obtained with the feed consisting of 20% graphite and 80% NMC by weight and the concentrator operated at 163 G force. The result showed that the recovery of NMC in the concentrate product decreased slightly with increasing feed mass, and the solid concentration in the slurry had a minor impact on the recovery of NMC in the concentrate product. However, the recovery of graphite in the concentrate product decreased at a more rapid rate with increasing the feed mass, resulting in a better separation performance. For instance, at 100 g of feed mass, the recovery of graphite in the concentrate product at 5% solid concentration reached 71.60%. The graphite recovery in the concentrate product decreased to 25.65% and 15.32% at 300 g and 500 g of the feed mass, respectively. The result showed that the recovery of graphite in the concentrate product at 10% solid concentration was higher than those obtained at 5% solid concentration. Therefore, the separation index increased with increasing feed masses from 100 g to 400 g, and decreased at feed masses of 500 g or above (Fig. 6b). With 400 g of the feed mass, the separation index (SI) reached a maximum of 67.75%. Fig. 6b shows the separation result between the NMC and graphite materials obtained at 10% solid concentration. The results showed that a 10% solid concentration slightly lowered the separation

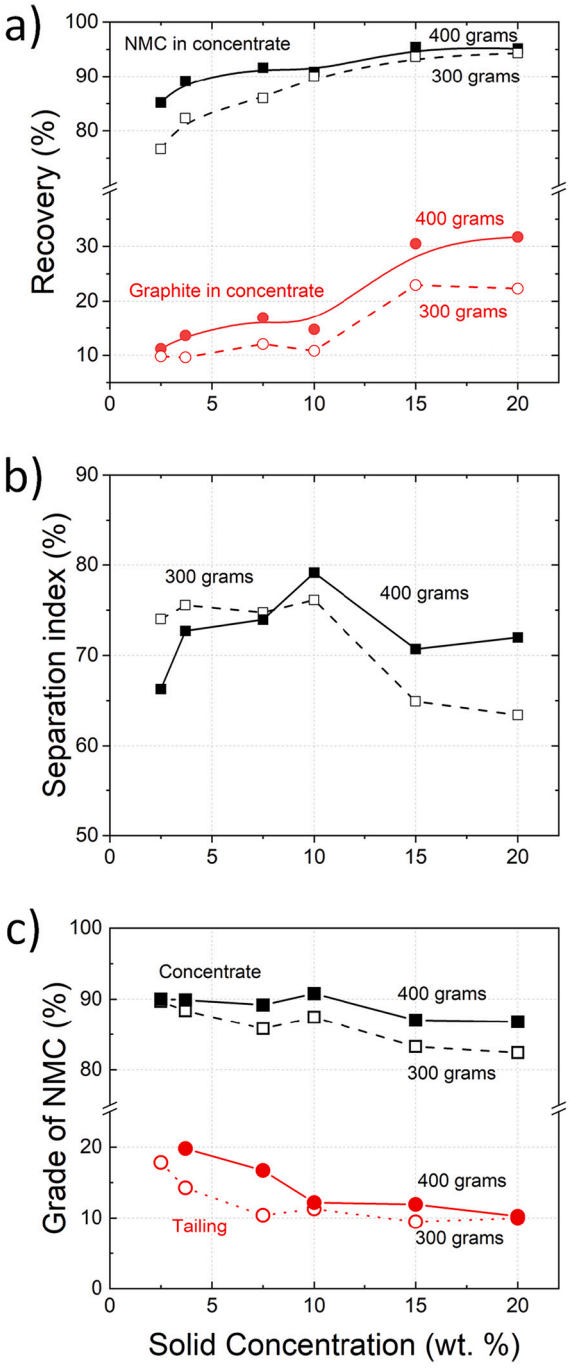

Fig. 5. Effect of solid concentration on the separation between the NMC and graphite. a) Recovery of NMC and graphite materials in the concentrate products with 300 g and 400 g of dry feed mass, b) separation index at different solid concentrations in the feed, and c) percentage (or grade) of NMC in the concentrate and tailing products.

performance compared to those obtained at 5% solid concentration in the feed slurry.

Fig. 7 shows the percentage of NMC in both the concentrate and the tailing products at different feed masses. It is desirable to have a low percentage of NMC in the tailing product to maximize the overall recovery. The result showed that the percentage of NMC in the concentrate product increased with increasing feed mass. With 300–400 g of dry feed, the percentage of NMC in the tailing product lowered to 3–5%, while the percentage of NMC in the concentrate product reached above 50%. Evidently, a 5% solid concentration achieved a better result in

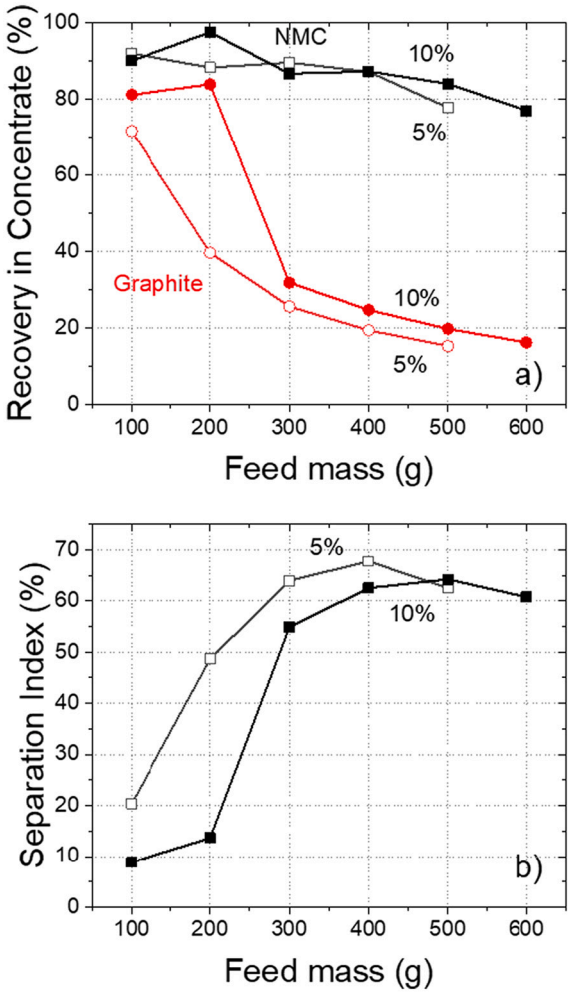

Fig. 6. Effect of feed mass and solid concentration on a) the recovery of NMC and graphite in the concentrate product b) separation index between the NMC and graphite from a blended mixture having a 20:80 NMC-to-graphite ratio by weight.

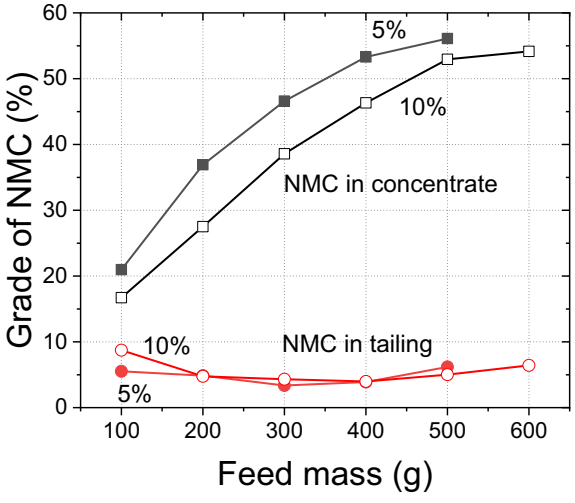

Fig. 7. Effect of feed mass and solid concentration on the grade of NMC in the concentrate and tailing products from a blended feed with 20:80 NMC-to-graphite ratio by weight.

maximizing the grade of NMC in the concentrate product and

minimizing the grade of NMC in the tailing product. A follow-up cleaning stage may be needed to further lower the percentage of NMC in the tailing product and maximize the overall recovery.

3.3. Multistage separation between pristine graphite and NMC

To increase the grade of NMC in the concentrate product and the grade of graphite in the tailing product, multiple stages of the gravity separation experiments were conducted. Fig. 8 shows a schematic drawing of a flowsheet that was used to evaluate the separation performance between the pristine NMC and graphite materials. The flowsheet (Fig. 8) consisted of a rougher stage, two sequential cleaner stages, and two sequential scavenger stages. In the rougher stage, the feed was fed to two separated circuits in parallel with 300 g of the dry feed in each run. Each run operated at 300 G force. Materials collected within the concentrator from the two parallel runs were combined and mixed with DI water to prepare a 5% solid slurry, which were then fed into a cleaner stage. The cleaner stage again operated at 300 G force. In the cleaner stage, the second sampling method was used. Wet materials from the middle-to-bottom sections of the UF concentrator were collected as the concentrate product to maximize the grade of NMC in the concentrate product. The concentrate product was mixed with DI water to prepare a 5% solid slurry. The slurry was then fed into a second cleaner stage. Both the tailing products from the cleaner stages were combined as the middling product.

The overflow slurry after the rougher stage was dewatered and mixed with 6 L of the process water to prepare a slurry with 5% solids by weight, which was then fed into the first scavenger stage. In the scavenger cycle, materials collected with the concentrator were reported as the concentrate product, while the overflow product was reported as the tailing product to maximize the recovery of heavy particles in the concentrate. The overflow product from the first scavenger stage was dewatered and mixed with 4 L of the process water to prepare a slurry which was then fed to a second scavenger stage. The overflow product was used as the final tailing product. Both the concentrate products from both the first and the second scavenger cycles were combined and reported as the middling product.

Table 3 shows the composition of the separated products after each separation stage. The feed consisted of approximately 60% by weight of NMC and 40% by weight of graphite. After one rougher stage, the concentrate product consisted of 87–90% of NMC and 10–13% of graphite. The tailing product consisted of 18–20% NMC and 80–82% graphite by weight. The concentrate product from the rougher stage was fed into two cleaner stages in series. After the first cleaner stage, the percentage (grade) of NMC in the concentrate product raised to 98.38%. The percentage (grade) of NMC was further raised to 99.40% after a second cleaner stage. The tailing product from the rougher stage was fed into two scavenger stages. The percentage of NMC in the tailing products was lowered to 3.88% and 0.35%, respectively, after two scavenger stages in sequence. The final tailing product contained 0.35% of NMC and 99.65% of graphite by weight. Fig. 9 shows SEM images of the final concentrate, final tailing products and the middling product. As shown, the concentrate product consisted of NMC materials only, and the tailing product consisted of graphite materials. The middling product can be recycled and fed back into the rougher stage; however, this circuit design will not be covered in this article.

Table 3
Material compositions of the separated products after each separation stage in the flowsheet shown in Fig. 8.

Process	NMC in Feed (%)	NMC in Concentrate (%)	NMC in Tailing (%)
1st Rougher - Run1	62.94%	89.94%	19.69%
1st Rougher - Run2	60.78%	87.79%	17.91%
1st Cleaner	88.11%	98.38%	64.31%
2nd Cleaner	98.66%	99.40%	95.07%
1st Scavenger	19.46%	45.35%	3.88%
2nd Scavenger	2.94%	6.63%	0.35%

3.4. Black mass separation from spent Li-ion batteries

Based on the successful separation results obtained with a mixture of pristine graphite and NMC111 as the feed, it is reasonable to assume that the separation of the black mass, *i.e.,* a mixture of the anode and cathode active materials, from spent Li-ion batteries behave similarly. To test this

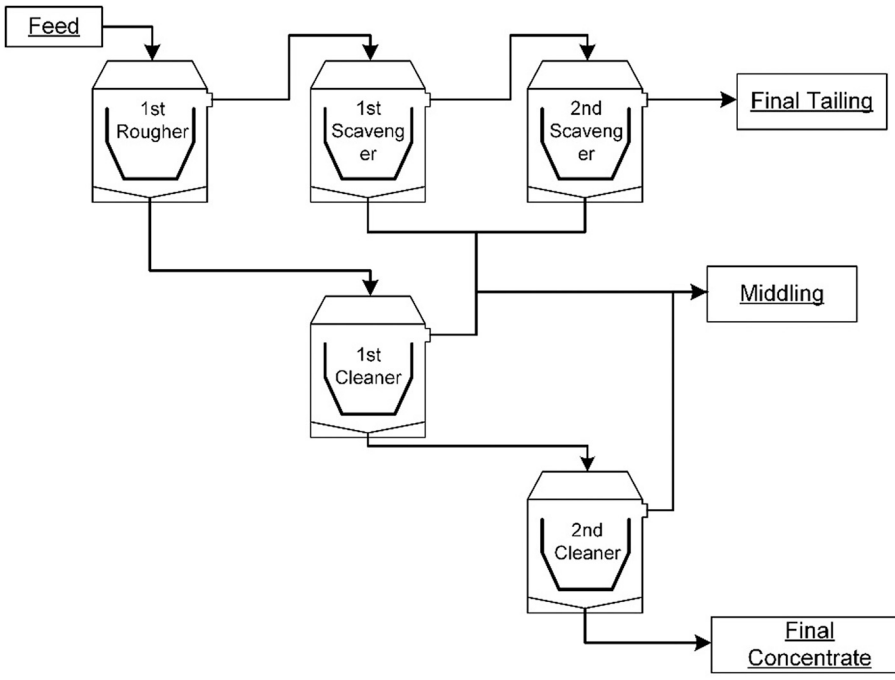

Fig. 8. A schematic drawing of the gravity separation circuit used to separate a mixture of pristine NMC and graphite powders.

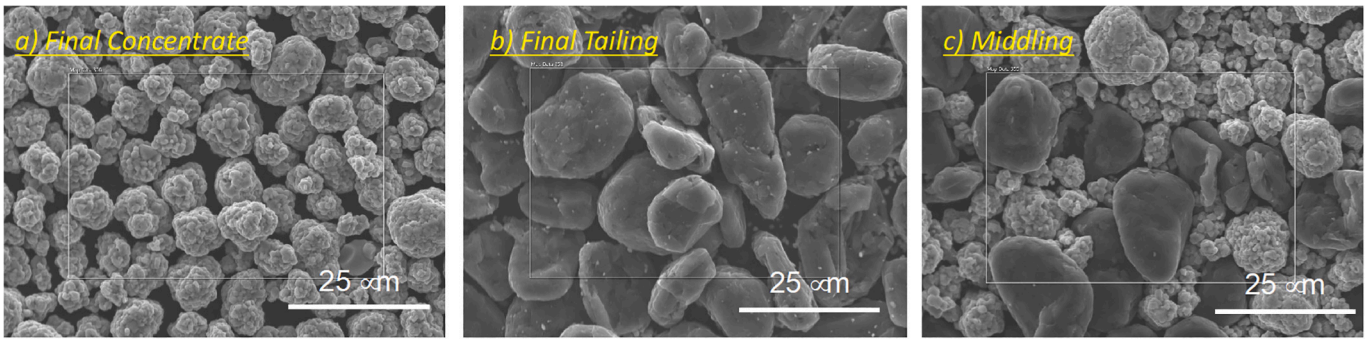

Fig. 9. SEM image of a) the concentrate product after the second cleaner cycle, b) the final tailing product after the second scavenger cycles, and c) the combined middling products from the process.

hypothesis, the separation of the black mass from spent Li-ion batteries was investigated using the Falcon Ultra-Fine (UF) gravity separator. Fig. 10a shows an SEM image of black mass obtained from spent cylinder LIBs. The detailed experimental procedure can be found in the experimental section of this article. As shown, both large agglomerates and individual electrode active materials were present in the black mass. Fig. 10b shows particle size distribution (PSD) of the black mass obtained from spent Li-ion batteries. The mean particle size (P50) was 20.2 μm. There was a small coarse fraction (>100 μm) in this sample, which were found to be PVDF-binded cathode agglomerates. The SEM data also revealed that graphite particles were found to be slightly bigger than cathode active materials from spent batteries. Furthermore, there were some micron-sized and sub-micron-sized particles in the feed, which were probably sourced from the cathode active materials.

Gravity separation experiments were conducted to separate the black mass from spent cylinder Li-ion batteries, and the result is shown in Fig. 11. Approximately 800 g of black mass materials in a 5 wt% solid

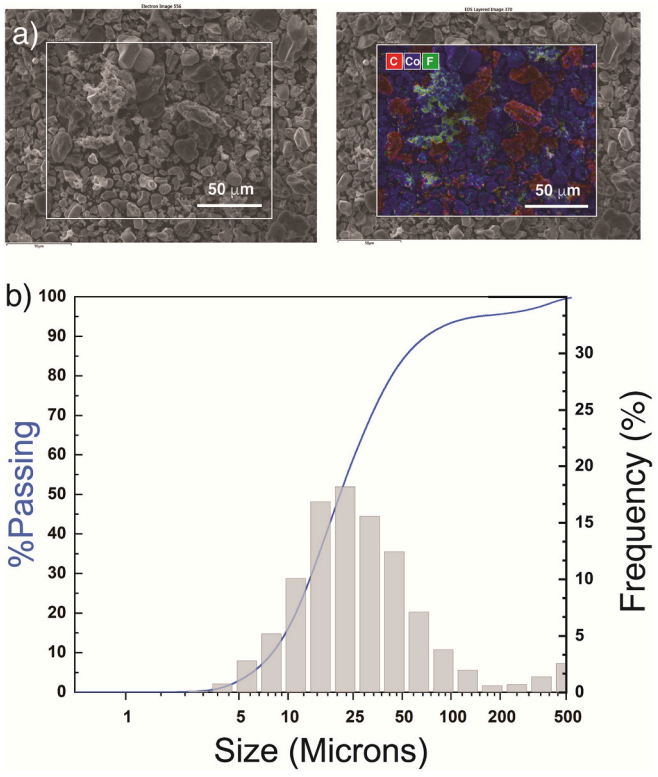

Fig. 10. a) SEM and EDX map of the black mass obtaineed from spent Li-ion batteries; b) particle size distribution (PSD) of the black mass from spent Li-ion batteries.

slurry were fed into two cycles in parallel. The concentrate products from two runs were combined and fed into the two cleaner stages in series. Fig. 11a shows a schematic flowsheet of a rougher-cleaner-recleaner circuit used in this part of the work. Fig. 11b shows both the yield and grade of lithium transition metal oxides (LTMOs) in the concentrate product after three stages of the gravity separation processes. The result showed that after one rougher stage, the percentage of lithium transition metal oxide (LTMO) in the concentrate product increased from 93.2% to 97.7% and 98.3% after first and second cleaner stages, respectively. On the contrary, the yield reduced from 61% to 40–50% after the first and second cleaner stages. Fig. 11c shows the weight loss as well as the derivative weight loss as a function of temperature for the concentrate products after 1) rougher, 2) cleaner, and 3) recleaner stages. There were three characteristic decomposition peaks at temperatures of ~280 °C, ~450 °C and ~ 600 °C, which represented an oxygen loss of LTMOs ($LiTMO_x$, $x < 2$) due to their thermal instability, decomposition of PVDF, and decomposition of graphite, respectively. It is evident that the $LiTMO_x$ peaks were ubiquitous in all three concentrate products, while both the PVDF and graphite peaks were diminished after the cleaner and recleaner stages. The result showed that after two recleaner stages, both the PVDF and graphite particles were rejected to the overflow stream.

To better understand the separation mechanism involved, SEM/EDX analyses of the separated products were conducted. Fig. 11d shows SEM and EDX mapping images of the tailing product after the rougher stage. As shown, both the graphite particles and PVDF-binded cathode agglomerates were reported to the tailing product. The presence of PVDF (ρ_{PVDF} = 1.78 g/cm^3) in these agglomerates effectively reduced the specific density of agglomerates, resulting in a rejection from the concentrator into the flushing overflow stream. Fig. 11e shows SEM and EDX images of the concentrate product after two cleaner stages. As shown, uniform and single cathode active materials were collected in the concentrate product. The percentage of LTMO materials in the concentrate product, as determined by the TGA method, exceeded 98%. Note that since the percentage of the LTMO materials in the separated products was determined by TGA, this percentage may be underestimated due to a slight weight loss associated with the thermal instability of the recycled lithium transition metal oxides from spent Li-ion batteries. The actual percentage of impurities (including PVDF, graphite, and carbon) in the final concentrate product should be less than 1%.

It should be noted that the yield of cathode active materials in the concentrate product was approximately 50%. As discussed above, PVDF-binded cathode agglomerates effectively reduced the cathode active material's specific gravity in water, resulting in a rejection of these cathode agglomerates in the overflow stream. One method to improve the yield is to recirculate the intermedia product into the rougher stage. By doing so, the yield may be increased by 10%–25%. An alternative method is to remove PVDF binders thermally [42], mechanically [43,44], or using solvents [45,46]. Detailed studies on these alternative

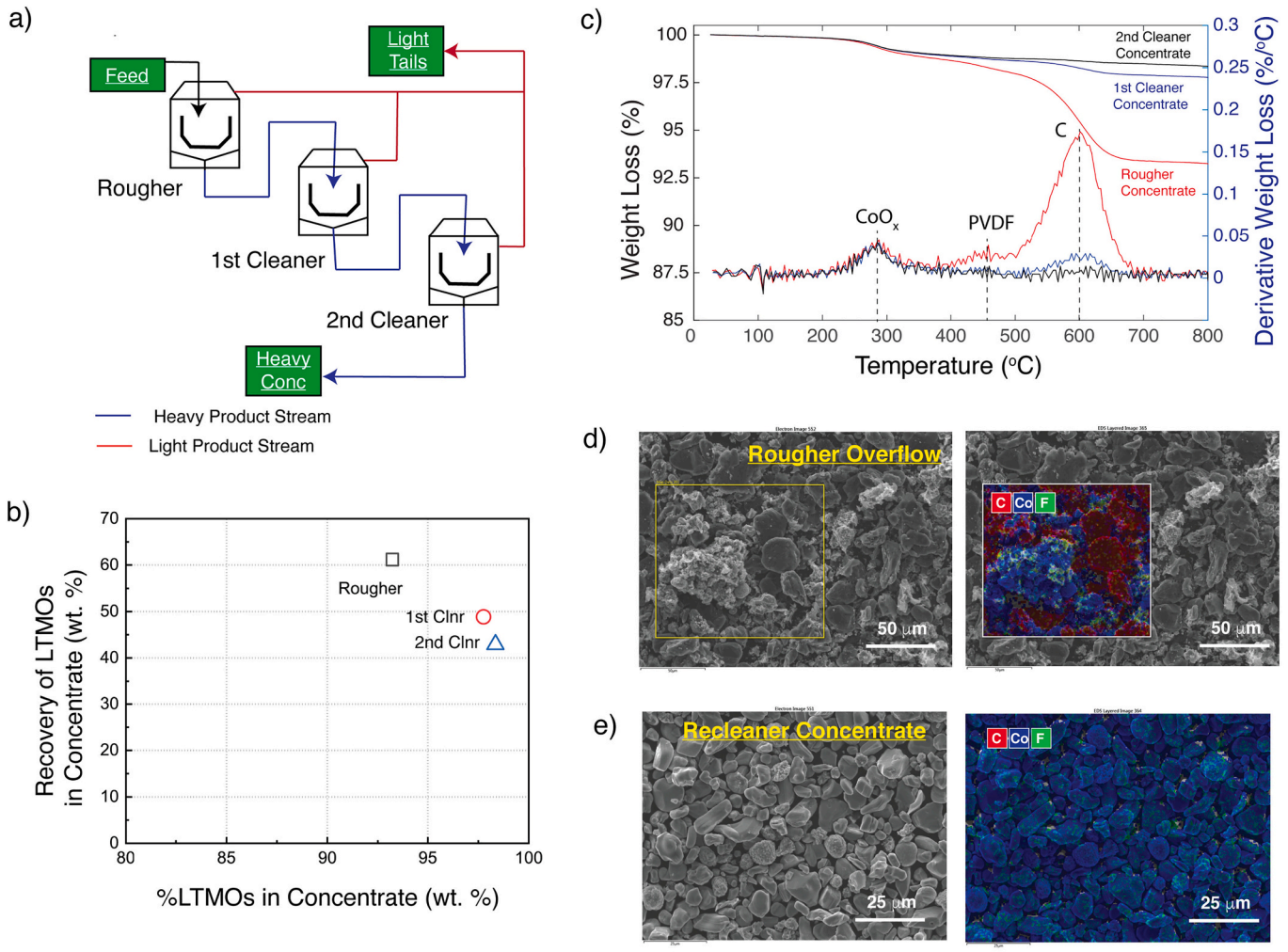

Fig. 11. a) A schematic flowsheet of the experimental circuit. b) Recovery *versus* grade of lithium transitional metal oxides (LTMOs) after three passes (rougher, cleaner and recleaner) in the UF concentrator. c) weight loss as well as derivative weight loss of the concentrate products; d) SEM and EDX mapping images of the tailing (overflow) product after the rougher stage; e) SEM and EDX images of the concentrate product after the 2nd cleaner stage.

methods will not be covered in this work. Nevertheless, the present result demonstrates a new method in separating ultrahigh purity cathode active materials from the black mass. These recycled high-purity cathode active materials may be reused directly after a relithiation and rejuvenation process.

4. Conclusions

Separation between the pristine graphite and NMC materials was evaluated using the Falcon Ultra-Fine (UF) concentrator. A series of experiments were conducted to study the effect of g-force, solid concentration, feed mass, and feed composition on the separation performance. The weight and composition of the separated products were analyzed to determine the separation index, which was then used to characterize separation performance. Results showed that both the feed mass and solid concentration impacted the separation performance significantly, with an optimum performance obtained at 400 g of dry feed and 5–10% solid concentration. It was also shown that the separation performance improved with increasing g-force. At 113 G or higher, the separation performance was less sensitive to the g-force. The present result also showed that the feed composition impacted the separation performance. For a feed having 20% NMC111 and 80% graphite by weight, the optimum separation was obtained at 5% solid concentration and 400 g of dry feed mass. The percentage of NMC in the tailing product after one pass in the UF concentrator was lowered to 3.89%. A multistage separation experiment was conducted with a final concentrate product consisted of 99% NMC111 and a final tailing product consisted of 99% graphite.

The Falcon UF gravity separation method was also extended to separate the electrode active materials in the black mass from spent cylinder Li-ion batteries. The result showed that after three passes in the Falcon UF concentrator, the grade of cathode active material in the concentrate product exceeded 98%, with no visual presence of anode active particles. The present result demonstrated an effective method for concentrating cathode active materials from the black mass from spent li-ion batteries and the ability to recycle high-purity cathode active materials from spent Li-ion batteries that can be regenerated for new battery application.

CRediT authorship contribution statement

Ruiting Zhan: Conceptualization, Methodology, Validation, Formal analysis, Investigation, Writing – original draft, Visualization. **Lei Pan:** Conceptualization, Resources, Writing – review & editing, Supervision.

Declaration of Competing Interest

The authors declare that they have no known competing financial

interests or personal relationships that could have appeared to influence the work reported in this paper.

Acknowledgement

The authors would like to acknowledge the financial support from the Department of Energy (DOE)'s Vehicle Technologies Office. Argonne National Laboratory is operated for DOE Office of Science by UChicago Argonne, LLC, under contract number DE-AC02-06CH11357. The U.S. government retains for itself, and others acting on its behalf, a paid-up nonexclusive, irrevocable worldwide license in said article to reproduce, prepare derivative works, distribute copies to the public, and perform publicly and display publicly, by or on behalf of the government. The authors would like to acknowledge Angelo Biviano for proofreading this manuscript.

References

[1] M. Armand, J.M. Tarascon, Building better batteries, Nature 451 (2008) 652–657.
[2] D. Larcher, J.M. Tarascon, Towards greener and more sustainable batteries for electrical energy storage, Nat. Chem. 7 (2014) 19–29.
[3] J.M. Tarascon, M. Armand, Issues and challenges facing rechargeable lithium batteries, Nature 414 (2001) 359–367.
[4] S. Maroufi, M. Assefi, R. Khayyam Nekouei, V. Sahajwalla, Recovery of lithium and cobalt from waste lithium-ion batteries through a selective isolation-suspension approach, sustainable, Mater. Technol. 23 (2020), e00139.
[5] E.A. Olivetti, G. Ceder, G.G. Gaustad, X. Fu, Lithium-ion battery supply chain considerations: analysis of potential bottlenecks in critical metals, Joule 1 (2017) 229–243.
[6] C. Xu, Q. Dai, L. Gaines, M. Hu, A. Tukker, B. Steubing, Future material demand for automotive lithium-based batteries, Commun. Mater. 1 (2020) 99.
[7] R. Sommerville, J. Shaw-Stewart, V. Goodship, N. Rowson, E. Kendrick, A review of physical processes used in the safe recycling of lithium ion batteries, Sustain. Mater. Technol. 25 (2020), e00197.
[8] L. Gaines, K. Richa, J. Spangenberger, Key issues for Li-ion battery recycling, MRS Energy Sust. 5 (2018) E14.
[9] G. Harper, R. Sommerville, E. Kendrick, L. Driscoll, P. Slater, R. Stolkin, A. Walton, P. Christensen, O. Heidrich, S. Lambert, A. Abbott, K. Ryder, L. Gaines, P. Anderson, Recycling lithium-ion batteries from electric vehicles, Nature 575 (2019) 75–86.
[10] A. Mayyas, D. Steward, M. Mann, The case for recycling: overview and challenges in the material supply chain for automotive li-ion batteries, Sustain. Mater. Technol. 19 (2019), e00087.
[11] L. Gaines, Lithium-ion battery recycling processes: research towards a sustainable course, Sust. Mater.Technol. 17 (2018), e00068.
[12] L. Gaines, The future of automotive lithium-ion battery recycling: charting a sustainable course, Sust. Mater.Technol. 1-2 (2014) 2–7.
[13] D.A. Bertuol, C. Toniasso, B.M. Jiménez, L. Meili, G.L. Dotto, E.H. Tanabe, M. L. Aguiar, Application of spouted bed elutriation in the recycling of lithium ion batteries, J. Power Sources 275 (2015) 627–632.
[14] H. Bi, H. Zhu, L. Zu, S. He, Y. Gao, S. Gao, Pneumatic separation and recycling of anode and cathode materials from spent lithium iron phosphate batteries, Waste Manag. Res. 37 (2019) 374–385.
[15] X. Zhong, W. Liu, J. Han, F. Jiao, H. Zhu, W. Qin, Pneumatic separation for crushed spent lithium-ion batteries, Waste Manag. 118 (2020) 331–340.
[16] Y. Bai, W.B. Hawley, C.J. Jafta, N. Muralidharan, B.J. Polzin, I. Belharouak, Sustainable recycling of cathode scraps via Cyrene-based separation, Sustain. Mater. Technol. 25 (2020), e00202.
[17] Y. Shi, G. Chen, Z. Chen, Effective regeneration of LiCoO2 from spent lithium-ion batteries: a direct approach towards high-performance active particles, Green Chem. 20 (2018) 851–862.
[18] S.E. Sloop, L. Crandon, M. Allen, M.M. Lerner, H. Zhang, W. Sirisaksoontorn, L. Gaines, J. Kim, M. Lee, Cathode healing methods for recycling of lithium-ion batteries, Sustain. Mater. Technol. 22 (2019).
[19] Y. Shi, M. Zhang, Y.S. Meng, Z. Chen, Ambient-pressure relithiation of degraded LixNi0.5Co0.2Mn0.3O2 ($0 < x < 1$) via eutectic solutions for direct regeneration of lithium-ion battery cathodes, Adv. Energy Mater. 9 (2019).
[20] J. Chen, Q. Li, J. Song, D. Song, L. Zhang, X. Shi, Environmentally friendly recycling and effective repairing of cathode powders from spent LiFePO4 batteries, Green Chem. 18 (2016) 2500–2506.
[21] X. Zhang, Q. Xue, L. Li, E. Fan, F. Wu, R. Chen, Sustainable recycling and regeneration of cathode scraps from industrial production of lithium-ion batteries, ACS Sustain. Chem. Eng. 4 (2016) 7041–7049.
[22] H. Nie, L. Xu, D. Song, J. Song, X. Shi, X. Wang, L. Zhang, Z. Yuan, LiCoO2: recycling from spent batteries and regeneration with solid state synthesis, Green Chem. 17 (2015) 1276–1280.
[23] R. Zhan, Z. Oldenburg, L. Pan, Recovery of active cathode materials from lithium-ion batteries using froth flotation, Sust. Mater.Technol. 17 (2018) e00062.
[24] R. Zhan, Z. Yang, I. Bloom, L. Pan, Significance of a solid electrolyte interphase on separation of anode and cathode materials from spent Li-ion batteries by froth flotation, ACS Sustain. Chem. Eng. 9 (2021) 531–540.
[25] G. Zhang, Y. He, H. Wang, Y. Feng, W. Xie, X. Zhu, Removal of organics by pyrolysis for enhancing liberation and flotation behavior of electrode materials derived from spent lithium-ion batteries, ACS Sustain. Chem. Eng. 8 (2020) 2205–2214.
[26] H. Shin, R. Zhan, K.S. Dhindsa, L. Pan, T. Han, Electrochemical performance of recycled cathode active materials using froth flotation-based separation process, J. Electrochem. Soc. 167 (2020), 020504.
[27] S.J. An, J. Li, C. Daniel, D. Mohanty, S. Nagpure, D.L. Wood, The state of understanding of the lithium-ion-battery graphite solid electrolyte interphase (SEI) and its relationship to formation cycling, Carbon 105 (2016) 52–76.
[28] J. Liu, H. Wang, T. Hu, X. Bai, S. Wang, W. Xie, J. Hao, Y. He, Recovery of LiCoO2 and graphite from spent lithium-ion batteries by cryogenic grinding and froth flotation, Miner. Eng. 148 (2020), 106223.
[29] H. Al-Shammari, S. Farhad, Regeneration of Cathode Mixture Active Materials Obtained from Recycled Lithium Ion Batteries, 2020. SAE Technical Paper.
[30] K.D. Kepler, F. Tsang, R. Vermeulen, P. Hailey, Processing for Recycling Electrode Materials from Lithium-Ion Batteries, US 2016/0072162, 2016.
[31] D. Munsterman, S. Kerstholt, Sodium polytungstate, a new non-toxic alternative to bromoform in heavy liquid separation, Rev. Palaeobot. Palynol. 91 (1996) 417–422.
[32] J. Callahan, A nontoxic heavy liquid and inexpensive filters for separation of mineral grains, J. Sediment. Res. 57 (1987) 765–766.
[33] Y. Zhang, Y. He, T. Zhang, X. Zhu, Y. Feng, G. Zhang, X. Bai, Application of falcon centrifuge in the recycling of electrode materials from spent lithium ion batteries, J. Clean. Prod. 202 (2018) 736–747.
[34] X.-N. Zhu, Y. Tao, Y.-Q. He, Y. Zhang, Q.-X. Sun, Pre-concentration of graphite and LiCoO2 in spent lithium-ion batteries using enhanced gravity concentrator, Physicochem. Prob. Min. Proc. 54 (2018) 293–299.
[35] Q. Dehaine, Y. Foucaud, J.S. Kroll-Rabotin, L.O. Filippov, Experimental investigation into the kinetics of falcon UF concentration: implications for fluid dynamic-based modelling, Sep. Purif. Technol. 215 (2019) 590–601.
[36] M.D. Adams, Summary of gold plants and processes, in, in: M.D. Adams, B.A. Wills (Eds.), Developments in Mineral Processing, Elsevier, 2005, pp. 994–1013.
[37] L.L. Coetzee, S.J. Theron, G.J. Martin, J.-D.V.D. Merwe, T.A. Stanek, Modern gold deportments and its application to industry, Miner. Eng. 24 (2011) 565–575.
[38] A. Gül, O. Kangal, A.A. Sirkeci, G. Önal, Beneficiation of the gold bearing ore by gravity and flotation, Int. J. Miner. Metall. Mater. 19 (2012) 106–110.
[39] S.A. McAlister, K.C. Armstrong, Development of the falcon concentrator, in: SME Annual Meeting, Society for Mining, Metallurgy, and Exploration, Orlando, Florida, 1998.
[40] J.-S. Kroll-Rabotin, É. Climent, F. Bourgeois, Beneficiation of concentrated ultrafine suspensions with a Falcon UF concentrator, Can. Instit. Min. J. 2 (2011) 189–198.
[41] L.O. Filippov, Q. Dehaine, I.V. Filippova, Rare earths (La, Ce, Nd) and rare metals (Sn, Nb, W) as by-products of kaolin production – part 3: processing of fines using gravity and flotation, Miner. Eng. 95 (2016) 96–106.
[42] Y. Yang, G. Huang, S. Xu, Y. He, X. Liu, Thermal treatment process for the recovery of valuable metals from spent lithium-ion batteries, Hydrometallurgy 165 (2016) 390–396.
[43] S.D. Widijatmoko, G. Fu, Z. Wang, P. Hall, Recovering lithium cobalt oxide, aluminium, and copper from spent lithium-ion battery via attrition scrubbing, J. Clean. Prod. 260 (2020), 120869.
[44] S.D. Widijatmoko, F. Gu, Z. Wang, P. Hall, Selective liberation in dry milled spent lithium-ion batteries, Sustain. Mater. Technol. 23 (2020), e00134.
[45] M. Contestabile, S. Panero, B. Scrosati, A laboratory-scale lithium-ion battery recycling process, J. Power Sources 92 (2001) 65–69.
[46] Y. Xu, D. Song, L. Li, C. An, Y. Wang, L. Jiao, H. Yuan, A simple solvent method for the recovery of LixCoO2 and its applications in alkaline rechargeable batteries, J. Power Sources 252 (2014) 286–291.